CMS Physics Analysis Summary

Contact: cms-pag-conveners-smp@cern.ch 2024/09/23

The strong coupling constant and its running from inclusive jet production at CMS

The CMS Collaboration

Abstract

A comprehensive analysis at next-to-next-to-leading order (NNLO) accuracy in quantum chromodynamics (QCD) is presented. It uses double-differential cross section measurements of inclusive jet production from the CMS Collaboration at centre-of-mass energies of 2.76, 7, 8, and 13 TeV. The result is a simultaneous determination of the value of the strong coupling constant at the mass of the Z boson $\alpha_s(M_Z)$ together with the parton distribution functions of the proton. The value $\alpha_s(M_Z) = 0.1176^{+0.0014}_{-0.0016}$ is obtained. By using the measurements in different intervals of jet transverse momenta, the running of the strong coupling is probed for energy scales between 100 and 1600 GeV.

1 Introduction

Collimated sprays of particles, conventionally called jets, are abundantly produced in high energy proton-proton (pp) collisions at the CERN LHC. At sufficiently high transverse momenta (p_T), jet production is described by quantum chromodynamics (QCD) using perturbative techniques (pQCD), which have now reached next-to-next-to-leading order (NNLO) accuracy.

Description of jet production in hadronic collisions depends on the value of the strong coupling constant α_S and an accurate understanding of the proton structure, encoded in the parton distribution functions (PDFs). Precise measurements of jet production provide a means to determine α_S at the mass of the Z boson $\alpha_S(m_Z)$ and the PDFs up to high values of x, which is the proton momentum fraction carried by the parton.

Inclusive jet production $pp \to \text{jet} + X$, refers to events with at least one jet with p_T above a certain threshold in the final state and is a key process to test pQCD calculations up to the highest accessible energy scales. In pp collisions at the LHC, inclusive jet production has been extensively studied by the CMS [1–6] and ATLAS [7–12] Collaborations at several centre-of-mass energies over a wide kinematic range.

This note presents results on PDFs and $\alpha_S(m_Z)$ obtained simultaneously from a comprehensive QCD analysis at NNLO, where the CMS measurements of inclusive jet production in pp collisions at $\sqrt{s} = 2.76$ [1], 7 [2, 3], 8 [4] and 13 TeV [5] are used together with cross section measurements of deep-inelastic scattering (DIS) at the DESY HERA [13]. In such a simultaneous extraction, the correlation between the PDFs and $\alpha_S(m_Z)$ is mitigated [14] to allow for an unbiased determination. Furthermore, the running of α_S as a function of the energy scale is demonstrated at NNLO up to 1.6 TeV.

2 Inclusive jet measurements

In this note, four CMS measurements of the double-differential inclusive jet cross section as a function of the individual jet p_T and absolute rapidity $|y|$ are considered. These measurements use jets clustered with the anti-k_T [15] algorithm as implemented in the FastJet [16] program with a distance parameter of $R = 0.7$. For each of the measurements, the corresponding integrated luminosity $\mathcal{L}$, the number of data points N_{dp}, and the ranges in p_T and $|y|$ are summarised in Tab. 1.

The primary source of experimental systematic uncertainty in jet measurements stems from the calibration of the jet energy scale (JES) and the jet energy resolution (JER). These calibrations and their associated uncertainties are determined using test beam data, Monte Carlo (MC) simulations, and samples of dijet, Z+jet, γ+jet and multijet production [17, 18]. The correlation of these uncertainties across the data points within an individual measurements and among

Table 1: The CMS inclusive jet measurements considered in this study. The columns show the $\sqrt{s}$, the integrated luminosity, the number of measured data points, the ranges of individual jet p_T and $|y|$, and the reference.

$\sqrt{s}$ [TeV]	$\mathcal{L}$ [fb^{-1}]	N_{dp}	p_T [GeV]	$\lvert y\rvert$	Ref.
2.76	0.0054	80	74–592	0.0–3.0	[1]
7	5.0	130	114–2116	0.0–2.5	[2, 3]
8	20	165	74–1784	0.0–3.0	[4]
13	33.5	78	97–3103	0.0–2.0	[5]

the measurements at different $\sqrt{s}$ were examined and are accounted for in the QCD analysis, as described in the following.

The JES uncertainties are subsumed into eight main categories.

- Uncertainties related to the absolute scale are associated with the JES correction within the barrel region, corresponding to pseudorapidities $|\eta| < 1.3$. This correction is obtained from a global fit using Z+jet, γ+jet, and multijet data, where extrapolations to higher p_{T} are performed by using MC simulations (*AbsoluteScale*). It includes a correction for initial-state and final-state radiation (ISR and FSR) (*AbsoluteMPFBias*). Additional uncertainties are introduced to address response differences from different MC event generators (*Fragmentation*) and the single-particle response in the electromagnetic calorimeter (ECAL) and in the hadronic calorimeter (HCAL) (*SinglePionECAL*, *SinglePionHCAL*).
- Relative JER uncertainties represent the η-dependent uncertainty from the JER corrections (*RelativeJER*).
- The relative η correction of the JES calibration results in a uniform detector response across different detector regions. It includes a log-linear p_{T} dependence. In addition, an uncertainty is included, associated with the procedure to derive this correction in different regions of the detector (*RelativePt*).
- Other relative contributions, such as *RelativeFSR*, correspond to uncertainties in the η-dependent corrections for ISR and FSR, and are summarised in an additional uncertainty.
- The statistical uncertainties in the determination of the relative corrections in different regions of η for different uncertainty sources are merged into one uncertainty (*RelativeStat*).
- Jet-flavour dependent uncertainties (*FlavourQCD*) encompass differences between data and MC simulations when applied to various jet flavour mixtures. The uncertainty is based on response differences to jets from uds/c/b-quarks and gluons between PYTHIA and HERWIG.
- Two time-dependent uncertainties address the JES variation over time during the data taking periods (*TimePt* and *TimeEta*).
- Uncertainties associated to the corrections for additional pp interactions within the same or nearby bunch crossings (pileup) are considered as well.

A detailed description of the JES calibration and the corresponding uncertainties is given in Refs. [17, 18]. Further uncertainties specific to each individual measurement are discussed in the original publications.

The following correlation scheme for JES-related uncertainties across the different CMS measurements is used in this analysis. For the measurement at $\sqrt{s} = 7$ TeV [2], the correlation scheme for JES-related uncertainties is used as described in Ref. [3]. In particular, the sources *SinglePionECAL* and *SinglePionHCAL* are decorrelated as a function of η. The uncertainties in pileup, the relative statistical contribution, and the time-dependent sources are considered uncorrelated between individual measurements. The *SinglePion* uncertainties in the 7 TeV data set are treated following the correlation scheme introduced in Ref. [3]. The JER uncertainties are treated as uncorrelated between the individual measurements. The correlations in the remaining JES uncertainties between different data sets are implemented as follows.

- The uncertainty *AbsoluteMPFBias* is correlated between the 2.76, 8, and 13 TeV mea-

surements. This uncertainty has not been considered for the 7 TeV measurement.

- The uncertainties in *AbsoluteScale*, *SinglePionECAL*, *SinglePionHCAL*, and *RelativeJER* are correlated between the 2.76 and 8 TeV measurements, because the corresponding corrections were obtained using 8 TeV data and applied to both measurements. These uncertainties are uncorrelated between the other data sets for which the corrections have been derived specifically.
- The *RelativeFSR* and *Fragmentation* uncertainties are fully correlated between the 2.76, 7, and 8 TeV measurements, but uncorrelated with the 13 TeV measurement, because of the use of different MC tunes and event generators for Run 1 and Run 2 data.
- The *RelativePt* uncertainties are uncorrelated between the individual measurements, since these reflect differences between linear and logarithmic fits in the p_{T} extrapolation of the residual corrections, different for the different years.
- The *FlavorQCD* uncertainty is treated correlated between the 7 and 8 TeV measurements, but uncorrelated with the 2.76 and 13 TeV measurements.

Different alternative correlation scenarios for the JES uncertainties were investigated and no significant impact on the results was observed, as quantified in Section 4.

While the JER uncertainties are uncorrelated across the measurements at different $\sqrt{s}$, the correlations of these uncertainties within each individual measurement have been investigated. In particular, the JER uncertainty is treated uncorrelated in $|y|$ for the measurements at 2.76, 7, and 8 TeV, because the residual $|y|$ dependence of these data sets was not fully accounted for. An additional uncorrelated uncertainty of 1.5% is assigned to the JER uncertainty in the 2.76 TeV measurement to take into account a statistical contribution to the JER uncertainty. Alternative JER uncertainty correlation scenarios are tested and lead to insignificant changes in the results.

3 Theoretical predictions

The NNLO pQCD calculations used in this study are performed assuming five active massless quark flavours in the leading-colour (LC) and leading-flavour-number approximation using the NNLOJET program [19]. The subleading colour contributions for the NNLO corrections, neglected in Ref. [19], have been recently calculated [20] and have a very small impact for inclusive jet production with $R = 0.7$. The renormalisation μ_{r} and factorisation μ_{f} scales in the calculation are set to the individual jet p_{T}, following the studies in Ref. [21]. The cross section predictions for bins in p_{T} and $|y|$ of the respective measurements are stored in the form of interpolation tables in the APPLFAST [22] format, allowing for a fast evaluation of the predictions under variations of α_{S}, PDFs, or the QCD scales. The numerical uncertainty in the grids is below 1% in most bins and increases to about 5% in the forward region at high p_{T}, remaining significantly smaller than the statistical uncertainties in the measurements. However, in the forward region at very high p_{T}, a few bins have grid uncertainties exceeding 10%, which are excluded from the QCD interpretation. As recommended by the authors of NNLOJET, the statistical uncertainties of the theory predictions are multiplied by a factor of two.

The QCD predictions are modified with a multiplicative correction for contributions of the dominant electroweak (EW) effects. These include Sudakov-type and other high-energy logarithms resulting from the virtual exchange of soft or collinear massive weak gauge bosons, calculated at next-to-leading order [23]. The contribution of EW effects becomes important at large jet p_{T}, reaching 11% at the highest p_{T} probed in the 13 TeV measurement. Subleading EW

effects from the emissions of a real weak gauge bosons have been estimated in the 13 TeV measurement to be smaller than 1% at high p_T and are neglected. The EW corrections for the 13 TeV measurement were taken from the original publication. For the 7 and 8 TeV measurements, these corrections have been updated by using more recent PDF sets. The EW corrections are omitted for the 2.76 TeV measurement because of their negligible impact for p_T smaller than 600 GeV.

To compare the fixed-order predictions to the measured particle-level cross sections, the predictions are corrected for the non-perturbative (NP) effects from hadronisation and the underlying event. These NP corrections have been derived as ratios from event generators with parton showers, in which NP effects are switched on and off. The NP corrections are applied through p_T- and $|y|$-dependent correction factors as provided in the original publications of the individual measurements. These use the generator tunes matching best the conditions of the corresponding measurements. The values of NP corrections vary between 5–20% at low p_T and decrease with increasing p_T. The associated uncertainties range from 2 to 4% at low p_T, depending on $|y|$, and are negligible at high p_T. Despite slight differences in the way the NP corrections were obtained for each measurement, the impact of the NP corrections in the QCD analysis is found to be insignificant considering their uncertainties. In particular, the impact of the NP corrections in the QCD analysis was studied by performing individual fits with a subset of measurements with $p_T > 150$, 200, and 300 GeV. This way, the kinematic ranges with decreasing importance of NP corrections are consequently probed. The difference in the results is found to be negligible. The main result is based on the full p_T spectra probed by the CMS jet data.

4 QCD analysis

In the QCD analysis, the four CMS measurements of the double-differential cross sections of inclusive jet production are used together with the combined neutral current (NC) and charged current (CC) ep DIS cross sections measured at the HERA collider at DESY [13].

Theoretical predictions for the DIS cross sections are calculated at fixed order in QCD at NNLO accuracy using the QCDNUM code [24], with μ_r and μ_f set to the squared four-momentum transfer Q^2. The contribution of massive c and b quarks in the DIS cross sections is treated in the Thorne-Roberts general-mass variable-flavour number scheme [25–27]. The masses of c and b quarks are set as $m_c = 1.47 \pm 0.06$ GeV and $m_b = 4.5 \pm 0.25$ GeV, respectively. The fraction of the strange quark in the sea $f_s = x\bar{s}/(x\bar{d} + x\bar{s})$ is assumed to be 0.4 ± 0.08. The low-Q^2 region in DIS, where resummation effects from small-x logarithms become important, is removed from the fit by using only the DIS measurements with $Q^2 > 10\,\text{GeV}^2$. This cut is varied by $2.5\,\text{GeV}^2$ up and down. The published DIS cross sections are already corrected by the dominant EW effects.

The PDFs for the gluon, valence u- and d-quark, and $\bar{u}$ and $\bar{d}$ quark densities are parametrized at a starting (evolution) scale of $Q_0^2 = 1.9\,\text{GeV}^2$, varied by $0.2\,\text{GeV}^2$. The Q^2 dependence of the PDFs and of α_S is obtained by solving the DGLAP evolution equations at NNLO in pQCD as implemented in QCDNUM. The functional form of the PDFs for each parton i at the starting scale is taken to be

$$xq_i(x) = A_i x^{B_i}(1-x)^{C_i} P_i(x) \tag{1}$$

where A is a normalization parameter and $P_i(x) = (1 + D_i x + E_i x^2)$ is a polynomial that interpolates between the small- and large-x behaviour given by the B and C parameters. The D and E terms in the polynomial expansion are only included following the results of an op-

Table 2: The values of χ^2 per number of degrees of freedom, N_{dof}, as obtained in the fit to HERA and CMS jet data. The partial χ^2 is reported for each of the individual datasets considered, together with the contribution to the χ^2 from correlated uncertainty sources.

Dataset	Partial χ^2/N_{dp}
HERA I+II neutral current	1036/935
HERA I+II charged current	112/81
CMS jets 2.76 TeV	63/80
CMS jets 7 TeV	81/130
CMS jets 8 TeV	206/165
CMS jets 13 TeV	77/78
Correlated χ^2	125
Total χ^2/N_{dof}	1680/1453

timization procedure. The parameters A_{u_v} and A_{d_v} are determined during the fit from the valence-quark number sum rule, while the value of A_g is obtained from the momentum sum rule. In the present work, the parametrization of the most recent NNLO QCD analysis [5] of the CMS measurement of inclusive jet production at 13 TeV is used. Further parameters are added, alternatively, to estimate the parametrization uncertainty.

The fit is performed using the xFITTER [28, 29] program. The values of the PDF parameters and of α_S are obtained in the minimization procedure using MINUIT [30] with a χ^2 goodness-of-fit (GoF) function that includes experimental and theoretical (PDF) uncertainties,

$$\chi^2(\mathbf{b}_{\text{exp}}, \mathbf{b}_{\text{th}}) = \sum_{i=1}^{N_{\text{data}}} \frac{\left[D_i - T_i(1 - \sum_j \gamma_{ij}^{\text{exp}} b_{j,\text{exp}})\right]^2}{\delta_{i,\text{uncor}}^2 T_i^2 + \delta_{i,\text{stat}}^2 D_i T_i} + \sum_i^{N_{\text{data}}} \log \frac{\delta_{i,\text{uncor}}^2 T_i^2 + \delta_{i,\text{stat}}^2 D_i T_i}{\delta_{i,\text{uncor}}^2 D_i^2 + \delta_{i,\text{stat}}^2 D_i^2} + \sum_{j=1}^{N_{\text{exp.sys}}} b_{j,\text{exp}}^2. \quad (2)$$

Here, D_i, T_i are the measurements and theory predictions, respectively. Further, $\delta_{i,\text{stat}}$, $\delta_{i,\text{uncor}}$ denote relative statistical and uncorrelated systematic uncertainties. The correlated uncertainty sources are accounted for by the $\mathbf{b}_{\text{exp}}$ set of parameters, with the impact of each source on the theory point σ_i^{exp} described by the matrices γ_{ij}^{exp}. Asymmetric uncertainties in the PDF parameters are obtained from a $\Delta\chi^2 = 1$ criterion using an iterative Hessian approach, following the prescription of Ref. [31]. The uncertainties quoted in the following, correspond to 68% confidence level (CL).

5 Results

In Fig. 1, the measurements are shown divided by the NNLO LC QCD predictions, corrected for the NP and EW effects. In general, a very good agreement between the theory predictions and the data is observed. The consistency of all the experimental data used is quantified by the goodness of the fit χ^2 from Eq. (2), presented in Tab. 2. The total χ^2 per number of data points N_{dp} is 1680/1453. A somewhat higher χ^2/N_{dp} for the HERA DIS data is investigated in detail in the original work [13]. The partial χ^2/N_{dp} of 427/453 is obtained for the CMS jet measurements.

In Fig. 2, the impact of the CMS jet data on the PDF extraction (*HERA+CMS* fit) is illustrated, considering the Hessian fit uncertainties. The fractional uncertainties in the PDFs resulting

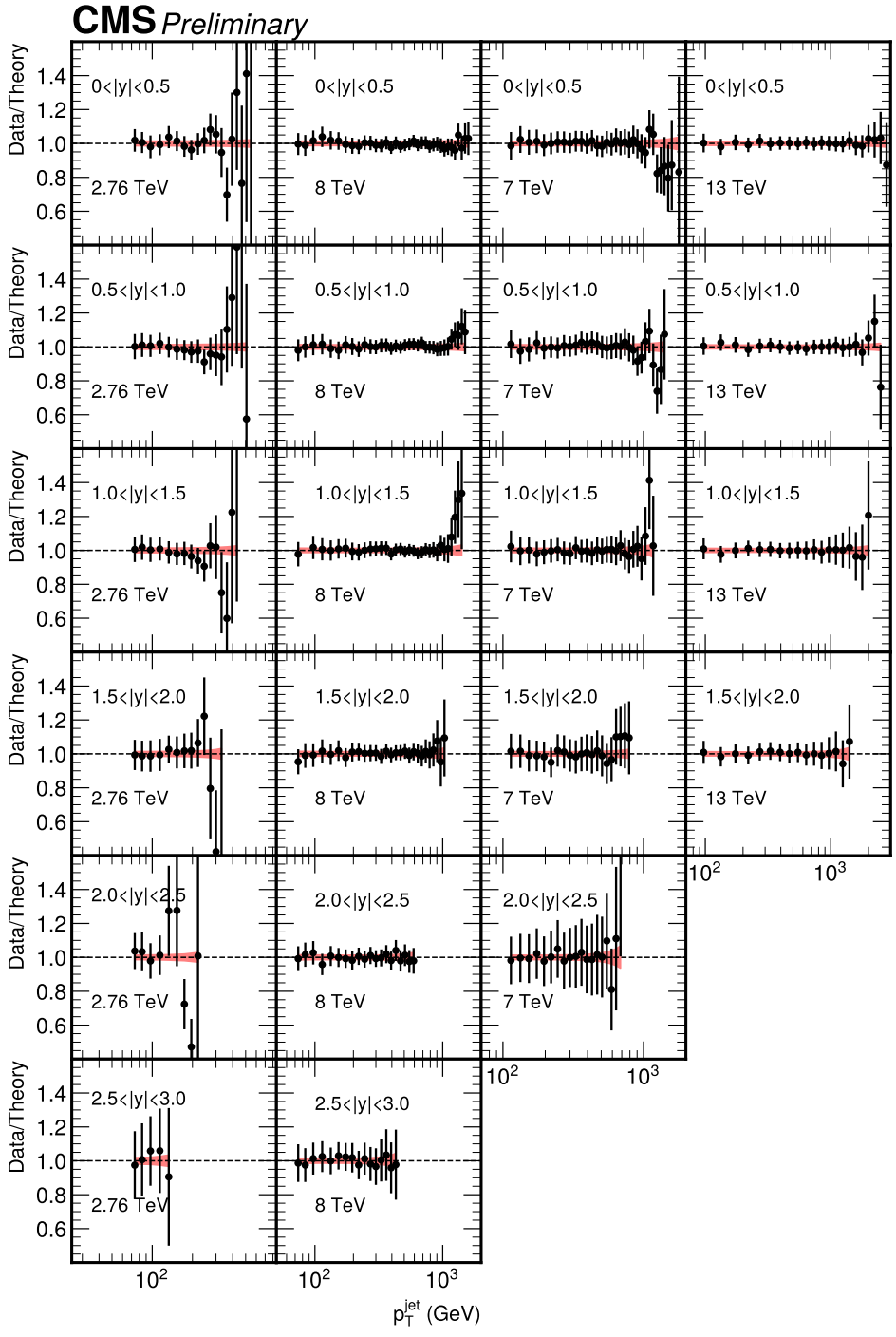

Figure 1: Cross sections of inclusive jet production in pp collisions as measured by CMS (black markers) at $\sqrt{s}$ of 2.76, 7, 8 and 13 TeV, using the anti-k_T clustering algorithm with $R = 0.7$, as a function of individual jet p_T in bins of absolute rapidity $|y|$. Shown is the total uncertainty of every data point (vertical bar). The data are divided by the NNLO LC QCD prediction corrected by the NP and EW effects. The PDFs obtained in this note are used. The total theory uncertainty (shaded band) includes the PDF and scale variation uncertainty.

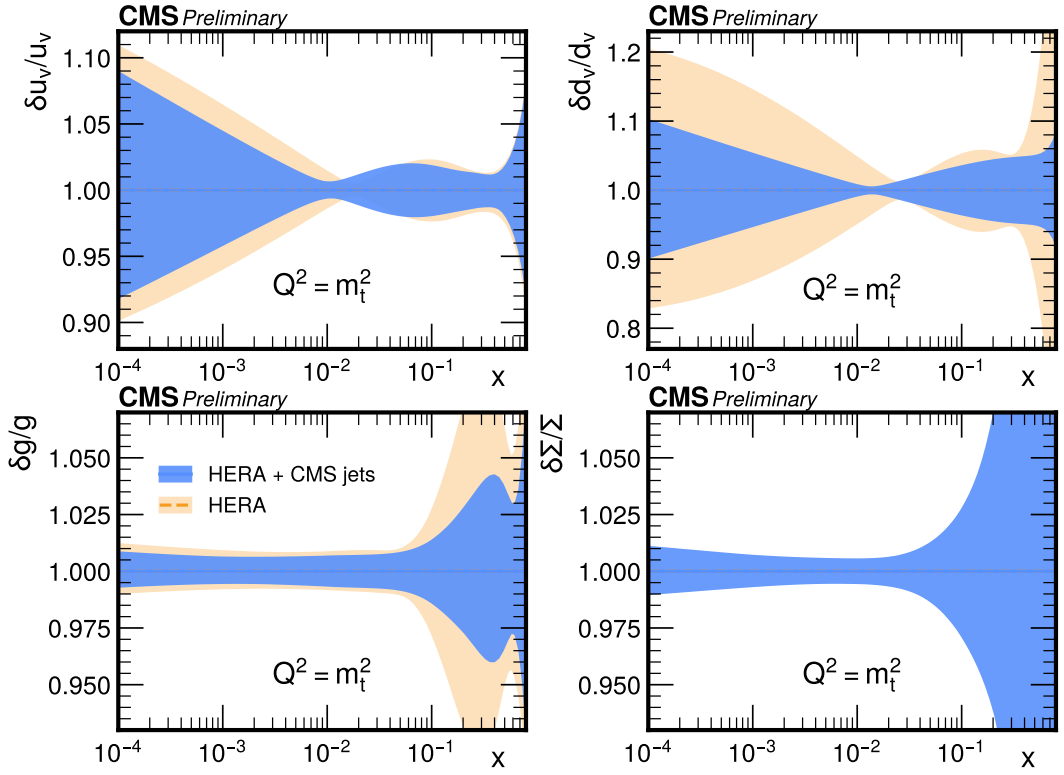

Figure 2: The fractional Hessian uncertainties in the u-valence u_v (upper left), d-valence d_v (upper right), gluon g (lower left), and sea quark Σ (lower right) distributions, shown as a function of x at the factorisation scale $Q^2 = m_t^2$. The results of the HERA+CMS fit (blue hatched area) are compared to the results of the HERA-only fit using $\alpha_S(m_Z) = 0.118$ (orange hatched area). The uncertainties are given at 68% CL.

from the present QCD analysis are shown in comparison to the results of an alternative fit which includes only HERA DIS data (*HERA-only* fit). In the HERA-only fit, due to poor sensitivity of the DIS data to $\alpha_S(m_Z)$, its value is fixed to the one of the HERA+CMS fit. The PDFs are shown at the factorization scale $Q^2 = m_t^2$, where m_t is the top quark mass. Significant improvement of the uncertainties in all PDFs is observed, once CMS jet measurements are considered.

In Fig. 3, the PDFs obtained in the HERA+CMS fit are compared to those obtained by the global fitting groups HERAPDF20 [13], NNPDF40 [33], CT18NNLO [32] and MSHT20 [34]. Note that these global PDFs are based on inclusive HERA DIS data and partially include the CMS jet measurements considered in the present note, except for the HERAPDF20 PDF set. By adding the CMS jet data, the valence PDF, in particular the d valence distribution, is observed to shift with respect to HERAPDF20 towards the results of the global PDFs, in particular NNPDF40 and MSHT20.

In the HERA+CMS fit, together with the PDFs, the value of the strong coupling at the m_Z is obtained as $\alpha_S(m_Z) = 0.1176 \pm 0.0009$, where the uncertainty denotes the Hessian fit uncertainties.

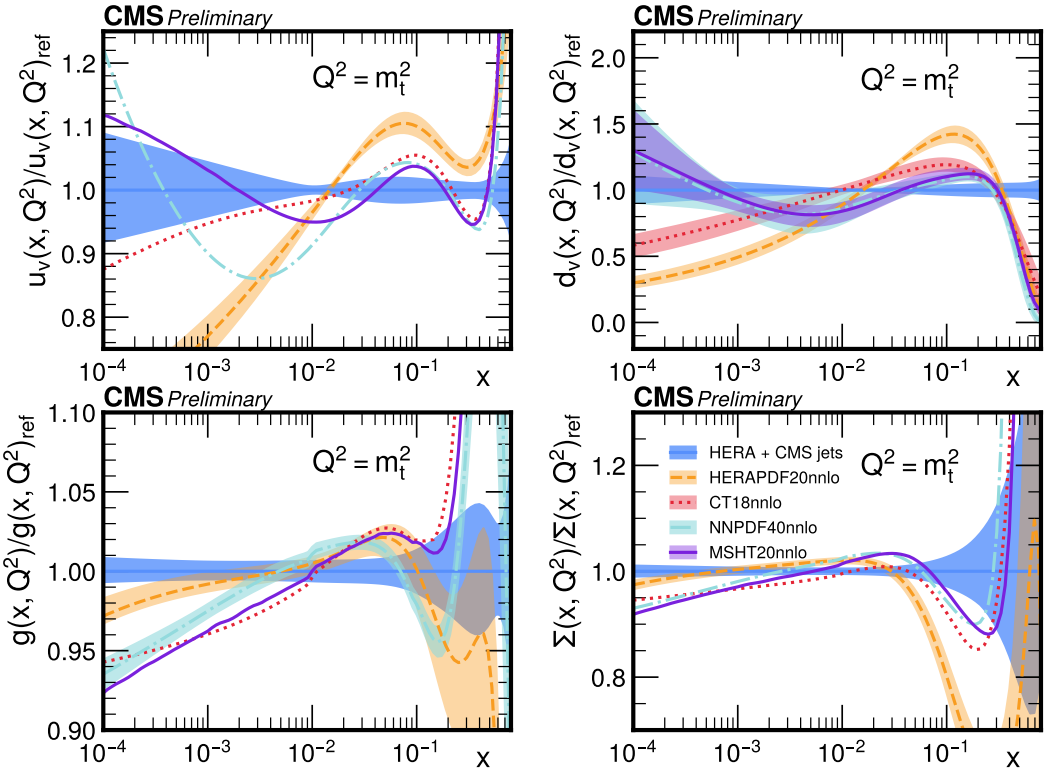

Figure 3: Ratios of different global PDF sets at NNLO, in particular CT18 [32], NNPDF4 [33], MSHT20 [34], and HERAPDF20 [13] to the result of the present study. The u-valence u_v (upper left), d-valence d_v (upper right), gluon g (lower left), and sea quark Σ (lower right) distributions are shown as functions of x at the factorisation scale $Q^2 = m_t^2$. The Hessian PDF uncertainties at 68% CL are shown.

Following the strategy of Ref. [5], further uncertainties in PDFs and $\alpha_S(m_Z)$ are considered, corresponding to the variations of the fit input parameters (*model uncertainty*), the uncertainty originating from missing higher-order corrections, and the one accounting for alternative parametrization shape (*parametrization uncertainty*). For every variation, an alternative fit is performed. The contributions to the model uncertainty are added in quadrature, resulting in $\delta\alpha_S(m_Z) = ^{+0.0006}_{-0.0004}$ (model). The uncertainty of missing higher orders in the calculation of the jet cross sections is evaluated by varying the scales μ_r and μ_f (*scale uncertainty*) independently by a factor of two up and down, avoiding cases with $\mu_f/\mu_r = 4$ or $1/4$. For each scale choice, an individual fit is performed, and the maximum difference to the central result is considered as an uncertainty of $\delta\alpha_S(m_Z) = ^{+0.0009}_{-0.0012}$ (scale). The parametrization uncertainty is estimated by extending the functional form of the PDFs by additional parameters D and E, added one at a time. An uncertainty $\delta\alpha_S(m_Z) = ^{+0}_{-0.00004}$ (param.) is obtained from an envelope of the results of the corresponding fits and is added linearly to the aforementioned uncertainties.

Summarising the findings above, the value of $\alpha_S(m_Z)$ is obtained as

$$\alpha_S(m_Z) = 0.11759^{+0.0009}_{-0.0009}\,(\text{fit})^{+0.0006}_{-0.0004}\,(\text{model})^{+0.0009}_{-0.0012}\,(\text{scale})^{+0.}_{-0.00004}\,(\text{param.}), \tag{3}$$

corresponding to the total uncertainty of $^{+0.0014}_{-0.0016}$ (tot). This value is in good agreement with

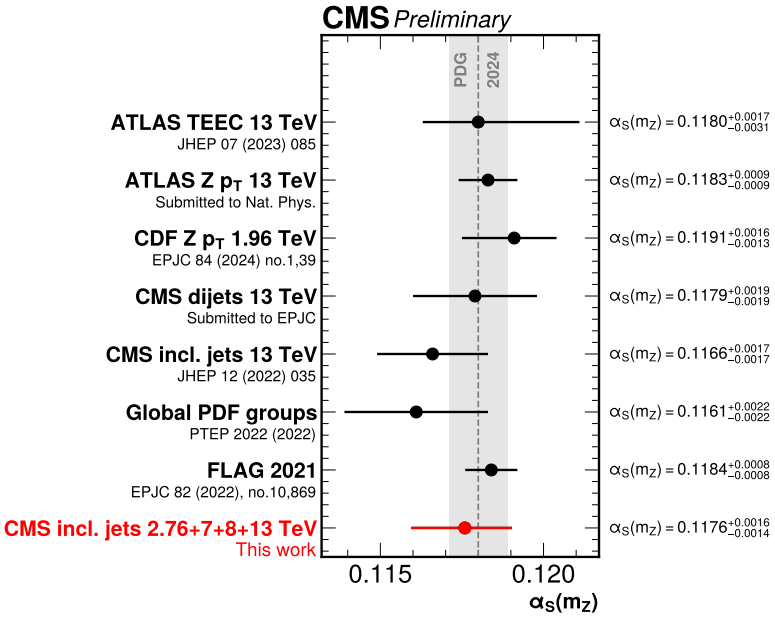

Figure 4: The value of $\alpha_S(m_Z)$ obtained in this analysis (red marker), compared to a selection of recent results obtained by using different methods (black markers) with their uncertainties (horizontal error bars). Also, the PDG world average is shown (shaded band).

previous determinations from hadron colliders, particularly with the CMS result based on a subset of the same data [5] and a dijet measurement at 13 TeV [35]. It also aligns well with the ATLAS measurement from the Sudakov peak of the Z-boson p_T [36] and transverse energy-energy correlations in multijet events [37], as well as the CDF result from the Z-boson p_T distribution [38]. Finally, the result agrees well with PDG category average of the global PDF fits [39], with the estimate from lattice QCD [40], and with the PDG world average of $\alpha_S(m_Z) = 0.1180 \pm 0.0009$ [39], as shown in Fig. 4. Applying alternative possible scenarios for the correlations of JES uncertainties between the data sets, mentioned in Section 2, resulted in a maximum shift in $\alpha_S(m_Z)$ of 0.41%, considered negligible compared to the fit uncertainty of 0.8% and the total uncertainty of 1.3%.

Following the same approach, the value of α_S in five different ranges of $\mu_r = p_T$ is extracted, illustrating the running of the strong coupling, $\alpha_S(\mu_r)$ at NNLO. For this purpose, the CMS measurements of inclusive jet production are split into exclusive ranges of individual jet p_T. In each independent p_T range, the PDFs and $\alpha_S(m_Z)$ are extracted simultaneously. The values of $\alpha_S(m_Z)$ obtained in each individual fit are evolved as $\alpha_S(\mu_r)$ using the five-loop five-flavour renormalization group equation (RGE) encoded in CRUNDEC [41] version 0.5.2. The same RGE is used to obtain the corresponding uncertainties. The fit, model, scale, and parametrization uncertainties are computed as in case of Eq. (3). In the estimate of the scale uncertainty, only variations in μ_f are considered, because the μ_r dependence is probed in this study. In each p_T range, μ_r is calculated at NNLO QCD as a cross section-weighted average $\langle p_T \rangle$. Results are summarised in Table 3 and shown in Fig. 5, where the values of $\alpha_S(\mu_r)$ are compared to the evolution of the world average of $\alpha_S(m_Z)$ performed at five-loop order in QCD using CRUNDEC [41].

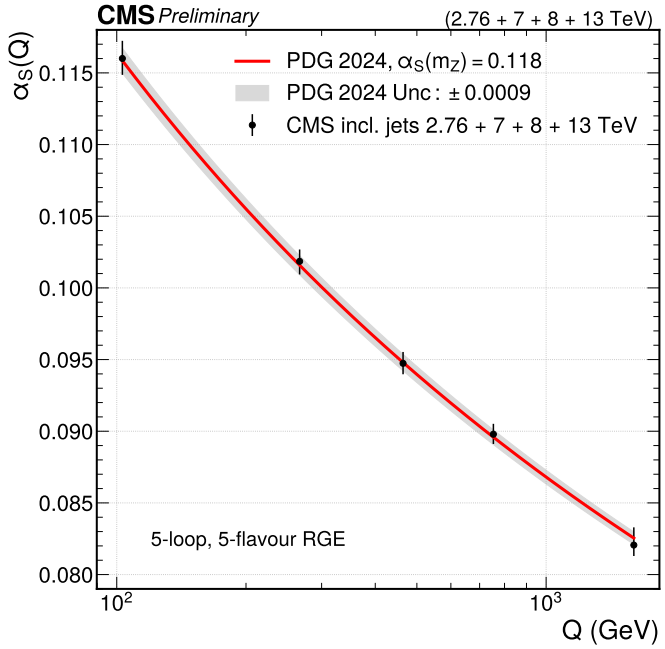

Figure 5: Values of α_S as a function of the renormalization scale, obtained in the present QCD analysis at NNLO. The results (black markers) are shown with their total uncertainties (vertical error bars). For comparison, the RGE at five loops is shown using the current world-average value $\alpha_S(m_Z) = 0.1180 \pm 0.0009$ [39] (red line) together with its associated total uncertainty (shaded band).

Table 3: The extracted $\alpha_S(m_Z)$ and the corresponding $\alpha_S(Q)$ values for each p_T range with their total uncertainties. For $\alpha_S(Q)$, the individual uncertainty contributions (fit, scale, model, parametrization) are listed.

p_T (GeV)	$\langle Q \rangle$	$\alpha_S(m_Z)$ (tot)	$\alpha_S(Q)$	(fit)	(scale)	(model)	(param.)	(tot)
74–220	103.06	$0.1182\ ^{+0.0013}_{-0.0012}$	0.1160	$^{+0.0011}_{-0.0011}$	$^{+0.000018}_{-0.00005}$	$^{+0.0006}_{-0.0004}$	$^{+0.0}_{-0.0}$	$^{+0.0012}_{-0.0011}$
220–395	266.63	$0.1184\ ^{+0.0011}_{-0.0012}$	0.1019	$^{+0.0007}_{-0.0007}$	$^{+0.0}_{-0.0004}$	$^{+0.0004}_{-0.00029}$	$^{+0.0}_{-0.000033}$	$^{+0.0008}_{-0.0009}$
395–638	464.31	$0.1179\ ^{+0.0012}_{-0.0012}$	0.0947	$^{+0.0007}_{-0.0007}$	$^{+0.0}_{-0.000032}$	$^{+0.0004}_{-0.00027}$	$^{+0.}_{-0.000008}$	$^{+0.0008}_{-0.0008}$
638–1410	753.66	$0.1184\ ^{+0.0013}_{-0.0012}$	0.0898	$^{+0.0006}_{-0.0006}$	$^{+0.0}_{-0.00004}$	$^{+0.0004}_{-0.00026}$	$^{+0.000005}_{-0.}$	$^{+0.0007}_{-0.0007}$
1410–3103	1600.5	$0.1170\ ^{+0.0020}_{-0.0016}$	0.0821	$^{+0.0007}_{-0.0007}$	$^{+0.0004}_{-0.0}$	$^{+0.0005}_{-0.00034}$	$^{+0.00004}_{-0.0}$	$^{+0.0010}_{-0.0008}$

6 Conclusions

The value of the strong coupling constant in the minimal subtraction scheme at the scale of the mass of the Z boson, $\alpha_S(m_Z)$, is extracted together with the parton distribution functions (PDFs) of the proton in an analysis at next-to-next-to-leading order (NNLO) in quantum chromodynamics (QCD). The analysis includes electroweak effects at next-to-leading order and non-perturbative corrections. The CMS measurements of inclusive jet production at $\sqrt{s} = 2.76$, 7, 8 and 13 TeV, using the anti-k_T clustering algorithm with a distance parameter of $R = 0.7$, are used together with the combined deep inelastic scattering (DIS) cross sections from HERA. The simultaneous extraction of $\alpha_S(m_Z)$ and the PDFs mitigates a possible bias from their correlations. By using the CMS jet data in the fit, the precision of PDFs is significantly improved and the value of $\alpha_S(m_Z) = 0.1176^{+0.0014}_{-0.0016}$ is obtained, in good agreement with the world average. It is the most precise measurement from jet cross sections, to date. Furthermore, by extracting the value of α_S in different bins of jet p_T, the running of α_S is tested at NNLO in QCD up to scales of 1.6 TeV. The observed running of α_S is in agreement with the prediction of the QCD renormalization group equation.

A JEC correlation of inclusive jet measurements

The JEC correlation scheme as illustrated in Fig. 6 has been applied in the QCD analysis of the CMS inclusive jet measurements at $\sqrt{s} = 2.76$, 7, 8, and 13 TeV. A filled black box indicates that the corresponding two uncertainty sources are treated as correlated.

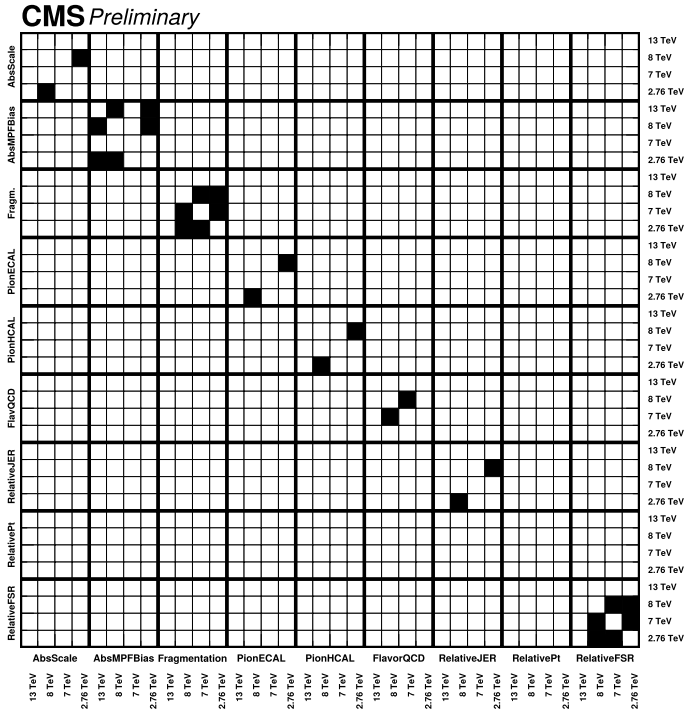

Figure 6: Sketch of the treatment of JES sources of uncertainty among the measurements at different $\sqrt{s}$. A filled black box indicates that the corresponding two uncertainty sources are treated as correlated.

References

[1] CMS Collaboration, "Measurement of the inclusive jet cross section in pp collisions at $\sqrt{s} = 2.76$ TeV", *Eur. Phys. J. C* **76** (2016) 265, doi:10.1140/epjc/s10052-016-4083-z, arXiv:1512.06212.

[2] CMS Collaboration, "Measurements of differential jet cross sections in proton-proton collisions at $\sqrt{s} = 7$ TeV with the CMS detector", *Phys. Rev. D* **87** (2013) 112002, doi:10.1103/PhysRevD.87.112002, arXiv:1212.6660. [Erratum: doi:10.1103/PhysRevD.87.119902].

[3] CMS Collaboration, "Constraints on parton distribution functions and extraction of the strong coupling constant from the inclusive jet cross section in pp collisions at $\sqrt{s} = 7$ TeV", *Eur. Phys. J. C* **75** (2015) 288, doi:10.1140/epjc/s10052-015-3499-1, arXiv:1410.6765.

[4] CMS Collaboration, "Measurement and QCD analysis of double-differential inclusive jet cross sections in pp collisions at $\sqrt{s} = 8$ TeV and cross section ratios to 2.76 and 7 TeV", *JHEP* **03** (2017) 156, doi:10.1007/JHEP03(2017)156, arXiv:1609.05331.

[5] CMS Collaboration, "Measurement and QCD analysis of double-differential inclusive jet cross sections in proton-proton collisions at $\sqrt{s} = 13$ TeV", *JHEP* **02** (2022) 142, doi:10.1007/JHEP02(2022)142, arXiv:2111.10431. [Addendum: doi:10.1007/JHEP12(2022)035].

[6] CMS Collaboration, "Measurement of the double-differential inclusive jet cross section in proton-proton collisions at $\sqrt{s}$ = 5.02 TeV", 2024. arXiv:2401.11355. Submitted to JHEP.

[7] ATLAS Collaboration, "Measurement of inclusive jet and dijet cross sections in proton-proton collisions at 7 TeV centre-of-mass energy with the ATLAS detector", *Eur. Phys. J. C* **71** (2011) 1512, doi:10.1140/epjc/s10052-010-1512-2, arXiv:1009.5908.

[8] ATLAS Collaboration, "Measurement of inclusive jet and dijet production in pp collisions at $\sqrt{s} = 7$ TeV using the ATLAS detector", *Phys. Rev. D* **86** (2012) 014022, doi:10.1103/PhysRevD.86.014022, arXiv:1112.6297.

[9] ATLAS Collaboration, "Measurement of the inclusive jet cross section in pp collisions at $\sqrt{s} = 2.76$ TeV and comparison to the inclusive jet cross section at $\sqrt{s} = 7$ TeV using the ATLAS detector", *Eur. Phys. J. C* **73** (2013) 2509, doi:10.1140/epjc/s10052-013-2509-4, arXiv:1304.4739.

[10] ATLAS Collaboration, "Measurement of the inclusive jet cross-section in proton-proton collisions at $\sqrt{s} = 7$ TeV using 4.5 fb^{-1} of data with the ATLAS detector", *JHEP* **02** (2015) 153, doi:10.1007/JHEP02(2015)153, arXiv:1410.8857. [Erratum: doi:10.1007/JHEP09(2015)141].

[11] ATLAS Collaboration, "Measurement of the inclusive jet cross-sections in proton-proton collisions at $\sqrt{s} = 8$ TeV with the ATLAS detector", *JHEP* **09** (2017) 020, doi:10.1007/JHEP09(2017)020, arXiv:1706.03192.

[12] ATLAS Collaboration, "Measurement of inclusive jet and dijet cross-sections in proton-proton collisions at $\sqrt{s} = 13$ TeV with the ATLAS detector", *JHEP* **05** (2018) 195, doi:10.1007/JHEP05(2018)195, arXiv:1711.02692.

[13] H1 and ZEUS Collaborations, "Combination of measurements of inclusive deep inelastic $e^{\pm}p$ scattering cross sections and QCD analysis of HERA data", *Eur. Phys. J. C* **75** (2015) 580, doi:10.1140/epjc/s10052-015-3710-4, arXiv:1506.06042.

[14] S. Forte and Z. Kassabov, "Why α_s cannot be determined from hadronic processes without simultaneously determining the parton distributions", *Eur. Phys. J. C* **80** (2020) 182, doi:10.1140/epjc/s10052-020-7748-6, arXiv:2001.04986.

[15] M. Cacciari, G. P. Salam, and G. Soyez, "The anti-k_T jet clustering algorithm", *JHEP* **04** (2008) 063, doi:10.1088/1126-6708/2008/04/063, arXiv:0802.1189.

[16] M. Cacciari, G. P. Salam, and G. Soyez, "FastJet User Manual", *Eur. Phys. J. C* **72** (2012) 1896, doi:10.1140/epjc/s10052-012-1896-2, arXiv:1111.6097.

[17] CMS Collaboration, "Jet energy scale and resolution in the CMS experiment in pp collisions at 8 TeV", *JINST* **12** (2017) P02014, doi:10.1088/1748-0221/12/02/P02014, arXiv:1607.03663.

[18] CMS Collaboration, "Determination of jet energy calibration and transverse momentum resolution in CMS", *JINST* **6** (2011) P11002, doi:10.1088/1748-0221/6/11/P11002, arXiv:1107.4277.

[19] J. Currie, E. W. N. Glover, and J. Pires, "Next-to-next-to leading order QCD predictions for single jet inclusive production at the LHC", *Phys. Rev. Lett.* **118** (2017) 072002, doi:10.1103/PhysRevLett.118.072002, arXiv:1611.01460.

[20] X. Chen et al., "NNLO QCD corrections in full colour for jet production observables at the LHC", *JHEP* **09** (2022) 025, doi:10.1007/JHEP09(2022)025, arXiv:2204.10173.

[21] J. Currie et al., "Infrared sensitivity of single jet inclusive production at hadron colliders", *JHEP* **10** (2018) 155, doi:10.1007/JHEP10(2018)155, arXiv:1807.03692.

[22] D. Britzger et al., "NNLO interpolation grids for jet production at the LHC", *Eur. Phys. J. C* **82** (2022) 930, doi:10.1140/epjc/s10052-022-10880-2, arXiv:2207.13735.

[23] S. Dittmaier, A. Huss, and C. Speckner, "Weak radiative corrections to dijet production at hadron colliders", *JHEP* **11** (2012) 095, doi:10.1007/JHEP11(2012)095, arXiv:1210.0438.

[24] M. Botje, "QCDNUM: Fast QCD evolution and convolution", *Comput. Phys. Commun.* **182** (2011) 490, doi:10.1016/j.cpc.2010.10.020, arXiv:1005.1481.

[25] R. S. Thorne and R. G. Roberts, "Ordered analysis of heavy flavor production in deep inelastic scattering", *Phys. Rev. D* **57** (1998) 6871, doi:10.1103/PhysRevD.57.6871, arXiv:hep-ph/9709442.

[26] R. S. Thorne, "Variable-flavor number scheme for NNLO", *Phys. Rev. D* **73** (2006) 054019, doi:10.1103/PhysRevD.73.054019, arXiv:hep-ph/0601245.

[27] R. S. Thorne, "Effect of changes of variable flavor number scheme on parton distribution functions and predicted cross sections", *Phys. Rev. D* **86** (2012) 074017, doi:10.1103/PhysRevD.86.074017, arXiv:1201.6180.

[28] S. Alekhin et al., "HERAFitter", *Eur. Phys. J. C* **75** (2015) 304, doi:10.1140/epjc/s10052-015-3480-z, arXiv:1410.4412.

[29] xFitter Developers' Team Collaboration, "xFitter 2.0.0: An Open Source QCD Fit Framework", *PoS* **DIS2017** (2018) 203, doi:10.22323/1.297.0203, arXiv:1709.01151.

[30] F. James and M. Roos, "Minuit: a system for function minimization and analysis of the parameter errors and correlations", *Comput. Phys. Commun.* **10** (1975) 343, doi:10.1016/0010-4655(75)90039-9.

[31] J. Pumplin et al., "Uncertainties of predictions from parton distribution functions. II. The Hessian method", *Phys. Rev. D* **65** (2001) 014013, doi:10.1103/PhysRevD.65.014013, arXiv:hep-ph/0101032.

[32] T.-J. Hou et al., "New CTEQ global analysis of quantum chromodynamics with high-precision data from the LHC", *Phys. Rev. D* **103** (2021) 014013, doi:10.1103/PhysRevD.103.014013, arXiv:1912.10053.

[33] NNPDF Collaboration, "The path to proton structure at 1% accuracy", *Eur. Phys. J. C* **82** (2022) 428, doi:10.1140/epjc/s10052-022-10328-7, arXiv:2109.02653.

[34] S. Bailey et al., "Parton distributions from LHC, HERA, Tevatron and fixed target data: MSHT20 PDFs", *Eur. Phys. J. C* **81** (2021) 341, doi:10.1140/epjc/s10052-021-09057-0, arXiv:2012.04684.

[35] CMS Collaboration, "Measurement of multidifferential cross sections for dijet production in proton-proton collisions at $\sqrt{s}$ = 13 TeV", 12, 2023. arXiv:2312.16669. Submitted to the European Physical Journal C.

[36] ATLAS Collaboration, "A precise determination of the strong-coupling constant from the recoil of Z bosons with the ATLAS experiment at $\sqrt{s} = 8$ TeV", 9, 2023. arXiv:2309.12986. Submitted to Nature Phys.

[37] ATLAS Collaboration, "Determination of the strong coupling constant from transverse energy−energy correlations in multijet events at $\sqrt{s} = 13$ TeV with the ATLAS detector", *JHEP* **07** (2023) 085, doi:10.1007/JHEP07(2023)085, arXiv:2301.09351.

[38] S. Camarda, G. Ferrera, and M. Schott, "Determination of the strong-coupling constant from the Z-boson transverse-momentum distribution", *Eur. Phys. J. C* **84** (2024) 39, doi:10.1140/epjc/s10052-023-12373-2, arXiv:2203.05394.

[39] Particle Data Group Collaboration, "Review of particle physics", *Phys. Rev. D* **110** (2024) 030001, doi:10.1103/PhysRevD.110.030001.

[40] Flavour Lattice Averaging Group (FLAG) Collaboration, "FLAG review 2021", *Eur. Phys. J. C* **82** (2022) 869, doi:10.1140/epjc/s10052-022-10536-1, arXiv:2111.09849.

[41] F. Herren and M. Steinhauser, "Version 3 of RunDec and CRunDec", *Comput. Phys. Commun.* **224** (2018) 333, doi:10.1016/j.cpc.2017.11.014, arXiv:1703.03751.